ARTICLE

Non-covalent Interaction of Heteroaromatic: Rotational Spectroscopy of the Thiazole-Formic Acid Complex†

Tingting Yang, Liuting Wang, Zhen Wang, Gang Feng*

School of Chemistry and Chemical Engineering, Chongqing University, Chongqing 401331, China

(Dated: Received on September 6, 2023; Accepted on October 13, 2023)

The characteristics of non-covalent linkages between thiazole and formic acid were explored by pulsed jet Fourier transform microwave spectroscopy supplemented with quantum chemical calculations. Rotational fingerprints of the thiazole···HCOOH and thiazole···HCOOD species were successfully measured in the supersonic expansion, both exhibiting ^{14}N quadrupole coupling hyperfine structure. The observed conformation has C_s symmetry, controlled by a predominant O−H···N hydrogen bond and an additional C−H···O hydrogen bond. The property of intermolecular non-covalent interactions emerging in the complex has been ulteriorly elucidated by implementing Johnson's non-covalent interaction analysis and the symmetry adapted perturbation theory analysis.

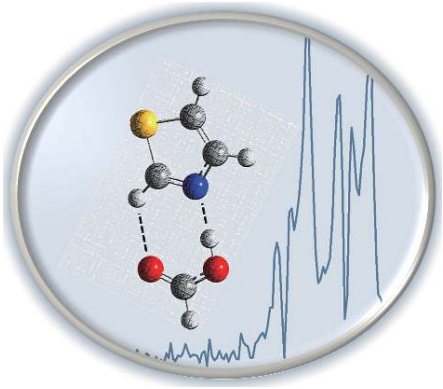

Key words: Rotational spectroscopy, Intermolecular weak interaction, Hydrogen bond, Aromatic interaction

I. INTRODUCTION

Aromatic heterocyclic scaffolds are diffusely distributed in nature and fundamentally important in biological chemistry. Many biological molecules such as proteins, coenzymes, alkaloids, as well as DNA, contain heteroaromatic scaffolds [1, 2]. Plenty of aromatic heterocyclic compounds, either natural or synthetic, are biologically and pharmacologically active [3, 4]. Comprehending the involved non-covalent interactions among those of proteins, nucleic acids, drugs, and their physical origins can contribute to explain the mechanism of intricate biological events [5–7]. Hydrogen bond (HB) stands for one of the most widespread and momentous non-covalent bonds participating in such biological processes.

Significant research effort has been devoted to uncovering the nature of hydrogen bonding formed between aromatic heterocycles and associated partners, revealing that the conjugated electronic structure of aromatic rings and heteroatom lone pairs are competitive sites in establishing non-covalent interaction (NCI) with the proton donor to form a hydrogen bond. For instance, in the water adducts of pyridine [8] and its derivatives [9–11], the nitrogen lone pair is the favored binding site leading to a primary O−H···N HB while one C−H···O_w HB further enhances its stability. A distinctly different bonding topology presents in pyrrole [12, 13] or indole [14] monohydrate, where the N−H···O contact prevails over the other weak interactions. The non-covalent bonding of selenophene [15] and thiophene [16–19] shows different behaviors, intending to form X−H···π (X=O, F, Cl or Br) HBs, probably due to the weak electronegativity of sulfur and selenium atoms. Similar features were observed in the benzofuran-H_2S complex [20]. The stabilization roles of various hydro-

† Part of Special Issue "In Memory of Prof. Qihe Zhu on the occasion of his 100th Anniversary".

* Author to whom correspondence should be addressed. E-mail: fengg@cqu.edu.cn

gen bonds in furan heterodimers with H_2O [21], HF [22], and HCl [23] were also characterized, in which the O/F/Cl–H···O HB determines its interaction pattern. However, in the complexes of furan with H_2S [24], PH_3 [24], and HBr [25], π-type HBs are favored. The formic acid (FA) shows similar bonding characteristics as water in forming complexes with thiophene, furan, and pyridine. The coplanar configuration constrained by O–H···N/O and C–H···O=C HBs is preferred in the pyridine-FA [26] and furan-FA [27] complexes, whereas the O–H···π HB is found to characterize the thiophene-FA [27] complex with the FA molecule located above the heterocyclic ring.

Thiazole (TZ), as a class of five-member heterocyclic motif containing one sulfur atom and one nitrogen atom, is the core scaffold of a range of drugs with multiple pharmacological activities [28–31]. The strength and properties of NCIs concerned in thiazole have been brought to the forefront. It was discovered that the O–H···N HB features the water complex with thiazole [32, 33]. Multiple interaction patterns were found for the TZ-formaldehyde [34] complex, either the n→π* or CH···N and CH···O stabilized conformations were detected. Most recently, rotational investigations revealed that thiazole links to CF_4 through a $N\cdots C_{CF_4}$ interaction and to SF_6 through the van der Waals interactions [35].

In this work, we combined Fourier transform microwave (FTMW) spectroscopy with quantum chemical computations to investigate the complex of FA and TZ. Rotational spectroscopic studies of model complexes can provide accurate structural information on the binding topologies without external interference from solvent and environment [36–38]. FA is taken as the partner because of its well-known proton acceptor and donor rules in building HBs. Therefore, the investigation of TZ-FA provides detailed structural information on the intermolecular interactions. The obtained results together with the previous reported ones enable a comprehensive comparison of the non-covalent bonding properties of TZ.

II. METHODS

A. Rotational spectroscopy

The target molecular complex was produced under supersonic expansion optimized for forming the TZ-FA dimer. Commercially available samples of FA (≥97%), TZ (≥98%), and deuterated water (D_2O, ≥98%) were used without additional treatment. The rotational spectrum was collected in the 2–20 GHz frequency region with a supersonic jet FTMW [39] spectrometer (coaxially oriented beam-resonator arrangement, COBRA-type) [40, 41].

Helium with a backing pressure of ~0.3 MPa was taken as the carrier gas and allowed to stream over a stainless-steel container filled with FA and TZ (at room temperature ~298 K) to seed the vapors. The mixed gas was injected into the Fabry-Pérot type cavity through the pulsed solenoid valve (0.5 mm nozzle diameter, Parker-General Valve), and polarized by short microwave pulse of specific frequencies. The molecular transient emission was collected and co-added for a total of at least 512 cycles, which was Fourier transformed to the frequency-domain spectrum. On account of the supersonic jet expanding coaxially along the resonator axis, each measured rotational transition appears as a doublet. The arithmetic mean of the two Doppler components is calculated as the ultimate transition frequency.

B. Quantum chemical computations

For assisting the spectral survey and assignment, the possible conformers of the TZ-FA complex were firstly explored computationally. Full geometry optimizations of all initial conformers were employed by using the B3LYP [42] method and the D3 [43] empirical dispersion corrections (Becke-Johnson damping function) [44] combined with the def2-TZVP [45] basis set. Carried out at the same level of theory, harmonic frequency calculations were done to confirm the obtained structures are the true energy minima and estimate the zero-point vibrational energy. The basis-sets superposition errors (BSSE) were considered in calculating the dissociation energies [46]. Furthermore, the Johnson's NCI [47] analysis was performed stemming from Multiwfn program [48] and VMD software [49] to character the non-covalent interactions appearing in the complex. Symmetry-adapted perturbation theory (SAPT) [50] analysis was conducted at the SAPT2+(3)δMP2/aug-cc-pVTZ level of theory utilizing the PSI4 program [51].

To assess the performance of different theoretical calculation methods in forecasting the equilibrium structure of TZ-FA for aiding rotational spectroscopic study, the derived most stable conformation was reoptimized at diverse levels. MP2 [52] and the density functional theory (DFT) methods including B2PLYP-D3(BJ), B3LYP-D3(BJ) and ωB97XD [53] combined with 6-311++G(d,p) [54], 6-311++G(2d,p), aug-cc-

DOI: 10.1063/1674-0068/cjcp2309082

TABLE I B3LYP-D3(BJ)/def2-TZVP calculated spectroscopic parameters of the two conformers (I and II) of TZ-FA. A, B, and C are rotational constants, χ_{aa} and $(\chi_{bb}-\chi_{cc})$ are the ^{14}N quadrupole coupling constants, and $|\mu_a|$, $|\mu_b|$, $|\mu_c|$ are the electric dipole moment components.

Conformer	A/MHz	B/MHz	C/MHz	$1.5\chi_{aa}$/MHz	$0.25(\chi_{bb}-\chi_{cc})$/MHz	$\|\mu_a\|$/D	$\|\mu_b\|$/D	$\|\mu_c\|$/D	P_{cc}/uÅ^2
I	4167	831	693	−4.83	−0.35	3.2	1.1	0.0	0.00
II	5006	759	659	−4.61	−0.44	3.4	0.7	0.0	0.00

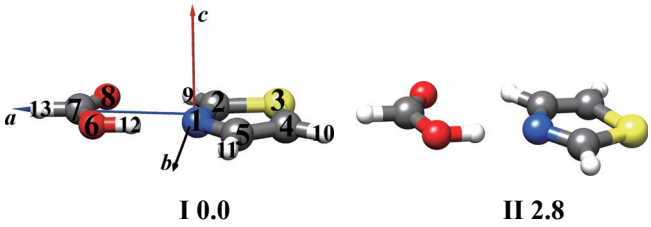

FIG. 1 Structures and the zero-point corrected relative energies (ΔE_0, in kJ/mol) of the two most stable conformers of TZ-FA predicted at the B3LYP-D3(BJ)/def2-TZVP level of theory.

pVTZ [55], and def2-TZVP basis sets, were employed using the Gaussian16 program package [56].

III. RESULTS AND DISCUSSION

A. Theoretical results

The theoretical calculations result in two low-energy conformers, as illustrated in FIG. 1, where the molecular structure, principal axes of inertia, atom labeling, and relative energies (ΔE_0) are provided. The calculated spectroscopic parameters and the planar moment of inertia P_{cc} ($=\sum m_i c_i^2$) are displayed in Table I. Both predicted conformers have C_s symmetry with FA located in the plane of TZ ring and are featured by an O−H···N HB and an additional C−H···O=C HB. The difference between the two conformers is that the carbonyl group of FA links with H9 (I) or H11 (II). Conformer II lies about 2.8 kJ/mol higher in energy than conformer I. This could be due to the fact that the positive electrostatic potential region of H9 of TZ monomer is larger than that of H11, being more likely to serve as a proton donor to build hydrogen bond as supported by the binding features of the TZ-water [32] and TZ-formaldehyde [34] complexes.

B. Rotational spectra

In accordance with the spectral pattern of the lowest energy conformer I, the preliminary spectral measurements were focused on the μ_a-type R-branch transitions in the frequency region from 8400 MHz to 9300 MHz, which was predicted to be the most intense

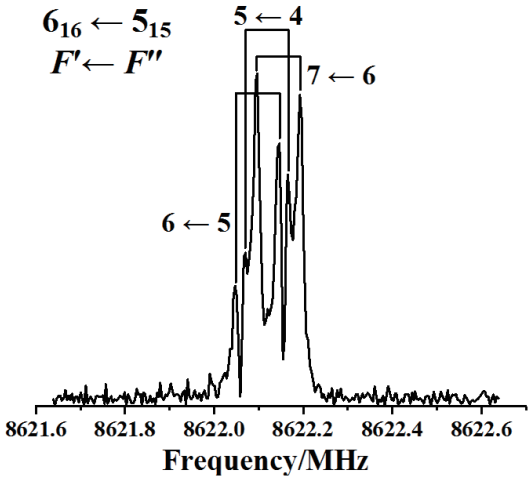

FIG. 2 The 6_{16}←5_{15} transition of the detected conformer displays the ^{14}N (I=1) nuclear quadrupole coupling hyperfine structure. The Doppler doubling arising from the COBRA setup is marked by "⊓".

branch. When the lines belonging to the TZ monomer and its monohydrate were removed from the observed spectra, the retained transitions were easily assigned with the help of the ^{14}N ($I=1$) nuclear hyperfine structure patterns. The $(J+1)$←J (6←5) transitions with $K_a=0$ and 1 were identified first and assigned to conformer I, as shown in FIG. 2. The measurements were further extended to 128 μ_a-type transitions of $J=4$–11 and $K_a=0$–3, as well as some weaker transitions of μ_b-type, so a set of spectroscopic constants could be well determined. However, none of μ_c-type transitions were detected in supersonic jets on account of the lack of μ_c dipole moment component resulting from planar symmetry. The assigned transition lines were fitted relying on the SPFIT program [57]. The semirigid-top Hamiltonian of Watson's S-reduced in I^r representation was chosen [58]. The spectroscopic parameters determined from the fit are summarized in Table II. It is straightforward to assign the experimentally determined conformation to conformer I with a maximum deviation of only about 1% by comparing the experimental rotational constant values with the computed ones.

Additionally, the rotational spectrum of one isotopologue (TZ-HCOOD) of the observed conformer was al-

DOI: 10.1063/1674-0068/cjcp2309082

TABLE II Experimental spectroscopic parameters of parent (TZ-HCOOH) and TZ-HCOOD species.

Species	A/MHz	B/MHz	C/MHz	$1.5\chi_{aa}$/MHz	$0.25(\chi_{bb}-\chi_{cc})$/MHz	D_J/kHz
TZ-HCOOH	4164.9422(3)[a]	822.4839(1)	687.21079(6)	−4.58(1)	−0.278(2)	0.1081(3)
TZ-HCOOD	4134.780(3)	817.8438(2)	683.15695(8)	[−4.58]	[−0.278]	[0.1081]

Species	D_{JK}/kHz	d_1/kHz	d_2/kHz	σ[b]/kHz	P_{cc}/uÅ^2	N[c]
TZ-HCOOH	0.345(6)	0.0198(2)	0.0014(2)	3.5	0.19	189
TZ-HCOOD	[0.345]	[0.0198]	[0.0014]	3.7	0.20	52

Note: centrifugal distortion constants are fixed at the values (in bracket) of the parent species.
[a] Errors in parentheses express the uncertainty of the last significant digit.
[b] Root-mean-square error of the fit.
[c] Number of the fitted transitions.

so determined by adding trace amounts of D_2O into the FA sample to induce the deuterium substitution reaction. This species was analyzed in the same way as the normal one, but only three rotational constants were allowed to be fitted and other parameters being fixed at the value of parent species because of a small number of rotational transition lines being observed. The resulting experimental parameters are available in Table II. All the assigned transition lines are listed in Table S2 and S3 of Supplementary materials (SM).

We have put effort to search rotational transition lines for conformer II but not succeed, presumably ascribed to the appearance of conformational relaxation or low populations in the supersonic expansion. Indeed, the conformational interconversion energy barrier between two lowest energy conformers has been computed at the B3LYP-D3(BJ)/def2-TZVP level of theory. The obtained result is displayed in FIG. S1 (SM), where the interconvertible barrier height from conformer II to the global minima is about 9.3 kJ/mol, much higher than the $2k_BT$ value in our case (~5.0 kJ/mol), and conformational relaxation could not occur. Therefore, the large factor for the non-detection of conformer II may be due to the very weak signals of the rotational transitions resulting in the missing of its assignment.

Rotational constants of the global minimum of the TZ-FA adduct calculated at the different levels of theory with deviations from the experimental values are shown in Table S1 (SM) and FIG. 3. The results indicate that the rotational constants obtained by B2PLYP-D3(BJ) method are more accurate than those obtained from ωB97XD, B3LYP-D3(BJ), and MP2 methods. In particular, rotational constants calculated at the B2PLYP-D3(BJ)/6-311++G(d,p) level are the closest to the experimental values, from which the mean absolute deviation is about 0.2%.

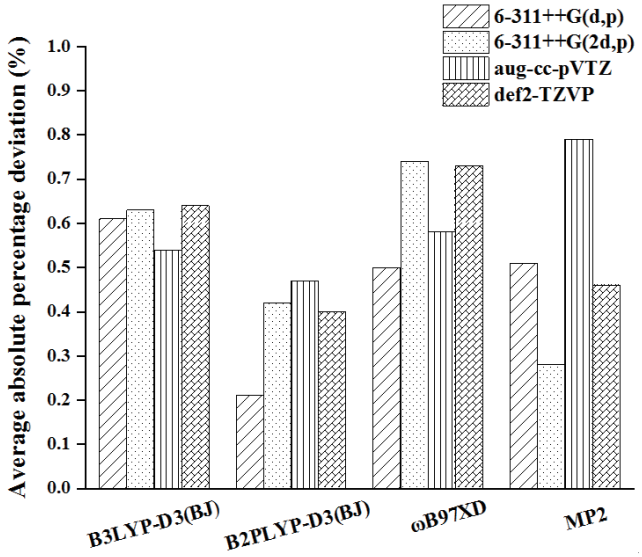

FIG. 3 Rotational constants of the global minimum of the TZ-FA adduct calculated at the different levels of theory with deviations from the experimental values.

C. Structures and intermolecular interactions

The Ray asymmetry parameter κ, $\kappa=(2B-A-C)/(A-C)$, acquired from three experimental rotational constants is −0.92, indicating the complex is approximately a prolate symmetric top. Table II reports that the experimental value of P_{cc} (about 0.2 uÅ^2) remains largely unchanged upon the deuteration of the hydrogen atom (HCOOD), signifying that the substituted hydrogen atom effectively locates in the ab plane.

Utilizing the STRFIT program [59], the effective structure (r_0) of the observed conformer was derived through a least-squared fit procedure to minimize the discrepancy between the theoretical and experimental rotational constants. The distance of N1O6 and the angle of ∠O6N1C5 were determined to be 2.76(1) Å and 135.1(8)° (Table III), respectively, while maintaining the remanent parameters at the theoretical values (r_e).

DOI: 10.1063/1674-0068/cjcp2309082

TABLE III The partial effective (r_0) and theoretical (r_e) values of the N1O6 distance and the ∠O6N1C5 angle.

Parameter	r(N1O6)/Å	∠O6N1C5/(°)
r_0	2.76(1)	135.1(8)
r_e	2.733	135.2

The substituted coordinates (r_s) of the hydrogen atom in the inertia principal axes system were also gained using the Kraitchman's equations, available in Table S4 (SM), and compared with the r_e and r_0.

The result from Jonson's NCI analysis is graphically reported in FIG. 4 to interpret the non-covalent linkages in the observed conformer. As depicted by the blue surface between the hydroxyl group and nitrogen atom, *i.e.*, the O−H···N HB, is the favored interaction. Another C−H···O=C interaction manifested green isosurface between the C7=O8 and the C2−H9 is also observed. The two non-covalent interactions close a seven-membered ring. The O−H···N HB is predicted to be stronger than C−H···O=C interaction.

Energy decomposition based on the SAPT analysis was employed to unambiguously comprehend the relative importance of the attractive and repulsive components, *i.e.*, dispersion (E_{disp}), induction (E_{ind}), electrostatics (E_{elec}), and exchange (E_{ex}). The calculational results of TZ-FA are listed in Table IV, compared with those for furan-FA [60], pyridine-FA [27] and thiophene-FA [60] calculated at the same theoretical level. The total interaction energy (E_{tot}) of TZ-FA (−57.7 kJ/mol) is close to that of pyridine-FA (−60.8 kJ/mol) but significantly stronger than that of thiophene-FA (−21.4 kJ/mol) and furan-FA (−30.7 kJ/mol), being consistent with the strength of N−H···O, O−H···π, and O−H···O HBs they formed, respectively. The largest stabilization terms of these complexes are all electrostatic interactions, accounting for at least 43% of the total attractive energy. But a noticeable enhancement is observed from the contributions of dispersion term, in the order of TZ-FA (19%) ≈ pyridine-FA (18%) < furan-FA (25%) < thiophene-FA (35%), which was opposite to the increase trend of the total energies. A similar situation holds for the monohydrates of furan, thiophene, thiazole and pyridine, while the stability of these complexes is significantly lower than that of the corresponding formic acid complexes.

D. Dissociation energy

The stretching motion of the detected conformer occurs nearly along the *a*-axis as indicated in FIG. 1, hence such motion could be detached from the rest of vibrational pattern in a first approximation. The pseudo-diatomic approximation [61] was adapted to estimate the force constant (k_s) through the formula:

$$k_s = 16\pi^4(\mu R_{CM})^2 \frac{4B^4 + 4C^4 - (B-C)^2(B+C)^2}{hD_J},$$

where μ, R_{CM} are the reduced mass and the distance between the centers of mass (R_{CM} = 4.217 Å) of the two subunits, respectively. B, C, and D_J values are the spectroscopic parameters of Table II. The value k_s=24.8 N/m corresponding to a harmonic stretch frequency of 118.8 cm^{-1} was roughly evaluated (see Table V). Whereafter, the dissociation energy D_0, $D_0 = k_s R_{CM}^2/72$, of TZ-FA was obtained to be ~36.9 kJ/mol through assuming a Lennard-Jones potential approximation which is close to the theoretical value (E_B, 49.5 kJ/mol) determined at the B3LYP-D3(BJ)/def2-TZVP level of theory. Table V also provides the dissociation energies of the complexes formed between FA with furan and pyridine using the same approximation. It is shown that the dissociation energy of TZ-FA is close to that of pyridine-FA (39.0 kJ/mol), but greater than those of furan-FA (32.0 kJ/mol).

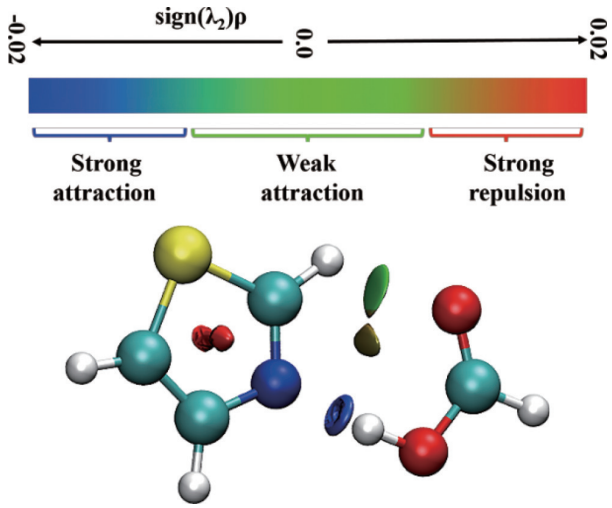

FIG. 4 The non-covalent interaction plot of the TZ-FA dimer.

IV. CONCLUSION

The TZ-FA complex was investigated using a combination of FTMW spectroscopy and quantum chemical calculations approach. Both observed rotational spectra of the parent (HCOOH) and the HCOOD species

DOI: 10.1063/1674-0068/cjcp2309082

TABLE IV The energy decomposition based on the SAPT analysis for TZ-FA, furan-FA, thiophene-FA and pyridine-FA. All energy values are given in kJ/mol, the contribution of E_{elec}, E_{ind}, and E_{disp} to the total attractive energy E_{tot} labeled in parathese.

Complex	E_{elec}	E_{ex}	E_{ind}	E_{disp}	E_{tot}
TZ-FA	−94.2 (55%)	114.4	−44.9 (26%)	−33.0 (19%)	−57.7
Furan-FA	−44.4 (53%)	53.7	−18.4 (22%)	−21.6 (25%)	−30.7
Thiophene-FA	−25.0 (43%)	36.4	−12.8 (22%)	−20.0 (35%)	−21.4
Pyridine-FA	−102.6 (54%)	128.8	−52.4(28%)	−34.6 (18%)	−60.8

TABLE V Distance between the centers of mass of two subunits R_{CM}, force constant k_s, and dissociation energies for the TZ-FA, furan-FA and pyridine-FA dimers (D_0 and E_B in kJ/mol).

Complex	R_{CM}/Å	k_s/(N/m)	D_0	E_B
TZ-FA	4.217	24.8	36.9	49.5
Furan-FA	4.410	19.7	32.0	24.9
Pyridine-FA	4.241	26.0	39.0	52.7

feature hyperfine structure derived from ^{14}N quadrupole coupling effect. The two subunits of TZ-FA form a planar seven-membered ring through one main O−H···N HB and an additional C−H···O=C HB. This preferred binding topology is similar to that of the corresponding pyridine adduct. The SAPT analysis further quantitatively discloses the importance of the electrostatic term for stabilizing the complex, accounting for 55% of the total attraction energy. The dissociation energy of the dimer is derived to be about 36.9 kJ/mol based on the pseudo-diatomic approximation model.

Supplementary materials: Potential energy curve relating to the interconversion of different conformers of TZ-FA (FIG. S1); theoretical spectroscopic parameters of the most stable conformation of the TZ-FA complex calculated at different levels of theory (Table S1); experimental transition frequencies of the TZ-HCOOH conformer I and the TZ-HCOOD isotope (Tables S2–S3); the r_s, r_0, and r_e coordinates of substituted atom D12 (Table S4) are available.

V. ACKNOWLEDGMENTS

This work was supported by the National Natural Science Foundation of China (No.22273009).

[1] K. E. Riley and P. Hobza, Acc. Chem. Res. **46**, 927 (2013).
[2] A. T. Balaban, D. C. Oniciu, and A. R. Katritzky, Chem. Rev. **104**, 2777 (2004).
[3] A. Al-Mulla, Der Pharma Chem. **9**, 141 (2017).
[4] M. S. Saini, A. Kumar, J. Dwivedi, and R. Singh, Int. J. Pharma Sci. Res. **4**, 66 (2013).
[5] S. Li, Y. Xu, Q. Shen, X. Liu, J. Lu, Y. Chen, T. Lu, C. Luo, X. Luo, M. Zheng, and H. Jiang, Curr. Pharm. Des. **19**, 6522 (2013).
[6] S. Jena, J. Dutta, K. D. Tulsiyan, A. K. Sahu, S. S. Choudhury, and H. S. Biswal, Chem. Soc. Rev. **51**, 4261 (2022).
[7] S. E. Wheeler and J. W. Bloom, J. Phys. Chem. A **118**, 6133 (2014).
[8] R. B. Mackenzie, C. T. Dewberry, R. D. Cornelius, C. J. Smith, and K. R. Leopold, J. Phys. Chem. A **121**, 855 (2017).
[9] X. Li, Y. Zheng, Q. Gou, G. Feng, and Z. Xia, J. Chem. Phys. **148**, 044306 (2018).
[10] W. Cheng, Y. Zheng, G. Feng, J. U. Grabow, and Q. Gou, Spectrochim. Acta Part A **239**, 118434 (2020).
[11] X. Wang, S. Gao, J. Chen, W. Du, W. Cheng, X. Xu, and Q. Gou, J. Phys. Chem. A **126**, 623 (2022).
[12] B. Wu, F. Xie, and Y. Xu, J. Mol. Spectrosc. **374**, 111381 (2020).
[13] M. J. Tubergen, A. M. Andrews, and R. L. Kuczkowski, J. Phys. Chem. **97**, 7451 (1993).
[14] S. Blanco, J. C. Lopez, J. L. Alonso, P. Ottaviani, and W. Caminàti, J. Chem. Phys. **119**, 880 (2003).
[15] J. J. Newby, T. Sivells, and A. N. Carney, J. Mol. Spectrosc. **389**, 111689 (2022).
[16] W. Silva and J. van Wijngaarden, J. Phys. Chem. A **125**, 3425 (2021).
[17] A. C. Legon and P. Ottaviani, Phys. Chem. Chem. Phys. **6**, 488 (2004).
[18] S. A. Cooke, G. K. Corlett, and A. C. Legon, J. Chem. Soc. Faraday Trans. **94**, 1565 (1998).
[19] S. A. Cooke, G. K. Corlett, and A. C. Legon, Chem. Phys. Lett. **291**, 269 (1998).
[20] Y. Jin, W. Li, R. T. Saragi, M. Juanes, C. Perez, A. Lesarri, and G. Feng, Phys. Chem. Chem. Phys. **25**, 12174 (2023).
[21] S. P. Lockwood, T. G. Fuller, and J. J. Newby, J. Phys. Chem. A **122**, 7160 (2018).
[22] A. Lesarri, J. C. López, and J. L. Alonso, J. Chem. Soc. Faraday Trans. **94**, 729 (1998).
[23] J. A. Shea and S. G. Kukolich, J. Chem. Phys. **78**,

3545 (1983).
[24] J. Y. Wu, J. C. Zhang, Z. X. Wang, and W. L. Cao, J. Chem. Phys. **127**, 175102 (2007).
[25] G. C. Cole, A. C. Legon, and P. Ottaviani, J. Chem. Phys. **117**, 2790 (2002).
[26] L. Spada, Q. Gou, B. M. Giuliano, and W. Caminati, J. Phys. Chem. A **120**, 5094 (2016).
[27] T. Yang, L. Wang, Z. Wang, Y. Xu, and G. Feng, J. Phys. Chem. A **126**, 4608 (2022).
[28] A. Ayati, S. Emami, S. Moghimi, and A. Foroumadi, Future Med. Chem. **11**, 1929 (2019).
[29] G. L. Khatik, A. K. Datusalia, W. Ahsan, P. Kaur, M. Vyas, A. Mittal, and S. K. Nayak, Curr. Drug Discovery Technol. **15**, 163 (2018).
[30] M. F. Arshad, A. Alam, A. A. Alshammari, M. B. Alhazza, I. M. Alzimam, M. A. Alam, G. Mustafa, M. S. Ansari, A. M. Alotaibi, A. A. Alotaibi, S. Kumar, S. M. B. Asdaq, M. Imran, P. K. Deb, K. N. Venugopala, and S. Jomah, Molecules **27**, 3994 (2022).
[31] Z. X. Niu, Y. T. Wang, S. N. Zhang, Y. Li, X. B. Chen, S. Q. Wang, and H. M. Liu, Eur. J. Med. Chem. **250**, 115172 (2023).
[32] W. Li, J. Chen, Y. Xu, T. Lu, Q. Gou, and G. Feng, Spectrochim. Acta Part A **242**, 118720 (2020).
[33] E. Gougoula, C. N. Cummings, Y. Xu, T. Lu, G. Feng, and N. R. Walker, J. Chem. Phys. **158**, 114307 (2023).
[34] W. Li, Y. Xu, Y. Jin, X. Li, W. Caminati, and G. Feng, Phys. Chem. Chem. Phys. **25**, 6491 (2023).
[35] T. Yang, Y. Xu, Z. Wang, C. Feng, and G. Feng, Phys. Chem. Chem. Phys. **25**, 25566 (2023).
[36] W. Caminati and J. U. Grabow, in *Frontiers and Advances in Molecular Spectroscopy*, J. Lanne Ed., Amsterdam: Elsevier, 569 (2018).
[37] M. Becucci and S. Melandri, Chem. Rev. **116**, 5014 (2016).
[38] M. Juanes, R. T. Saragi, W. Caminati, and A. Lesarri, Chem. Eur. J. **25**, 11402 (2019).
[39] *72nd International Symposium on Molecular Spectroscopy*, TH03, (2017).
[40] J. -U. Grabow and W. Stahl, Z. Naturforsch. A **45**, 1043 (1990).
[41] J. -U. Grabow, W. Stahl, and H. Dreizler, Rev. Sci. Instrum. **67**, 4072 (1996).
[42] A. D. Becke, J. Chem. Phys. **98**, 5648 (1993).
[43] S. Grimme, J. Comput. Chem. **27**, 1787 (2006).
[44] S. Grimme, S. Ehrlich, and L. Goerigk, J. Comput. Chem. **32**, 1456 (2011).
[45] F. Weigend and R. Ahlrichs, Phys. Chem. Chem. Phys. **7**, 3297 (2005).
[46] S. F. Boys and F. Bernardi, Mol. Phys. **19**, 553 (1970).
[47] E. R. Johnson, S. Keinan, P. Mori-Sánchez, J. Contreras-García, A. J. Cohen, and W. Yang, J. Am. Chem. Soc. **132**, 6498 (2010).
[48] T. Lu and F. Chen, J. Comput. Chem. **33**, 580 (2012).
[49] W. Humphrey, A. Dalke, and K. Schulten, J. Mol. Graphics **14**, 33 (1996).
[50] T. M. Parker, L. A. Burns, R. M. Parrish, A. G. Ryno, and C. D. Sherrill, J. Chem. Phys. **140**, 094106 (2014).
[51] R. M. Parrish, L. A. Burns, D. G. Smith, A. C. Simmonett, A. E. DePrince III, E. G. Hohenstein, U. Bozkaya, A. Y. Sokolov, R. Di Remigio, and R. M. Richard, J. Chem. Theory Comput. **13**, 3185 (2017).
[52] C. Møller and M. S. Plesset, Phys. Rev. **46**, 618 (1934).
[53] S. Grimme, J. Chem. Phys. **124**, 034108 (2006).
[54] J. D. Chai and M. Head-Gordon, Phys. Chem. Chem. Phys. **10**, 6615 (2008).
[55] M. J. Frisch, J. A. Pople, and J. S. Binkley, J. Chem. Phys. **80**, 3265 (1984).
[56] R. A. Kendall, T. H. Dunning Jr., and R. J. Harrison, J. Chem. Phys. **96**, 6796 (1992).
[57] M. J. Frisch, G. W. Trucks, H. B. Schlegel, G. E. Scuseria, M. A. Robb, J. R. Cheeseman, G. Scalmani, V. Barone, G. A. Petersson, H. Nakatsuji, X. Li, M. Caricato, A. V. Marenich, J. Bloino, B. G. Janesko, R. Gomperts, B. Mennucci, H. P. Hratchian, J. V. Ortiz, A. F. Izmaylov, J. L. Sonnenberg, D. Williams-Young, F. Ding, F. Lipparini, F. Egidi, J. Goings, B. Peng, A. Petrone, T. Henderson, D. Ranasinghe, V. G. Zakrzewski, J. Gao, N. Rega, G. Zheng, W. Liang, M. Hada, M. Ehara, K. Toyota, R. Fukuda, J. Hasegawa, M. Ishida, T. Nakajima, Y. Honda, O. Kitao, H. Nakai, T. Vreven, K. Throssell, J. A. Montgomery, Jr., J. E. Peralta, F. Ogliaro, M. J. Bearpark, J. J. Heyd, E. N. Brothers, K. N. Kudin, V. N. Staroverov, T. A. Keith, R. Kobayashi, J. Normand, K. Raghavachari, A. P. Rendell, J. C. Burant, S. S. Iyengar, J. Tomasi, M. Cossi, J. M. Millam, M. Klene, C. Adamo, R. Cammi, J. W. Ochterski, R. L. Martin, K. Morokuma, O. Farkas, J. B. Foresman, and D. J. Fox, *Gaussian16, Revision A. 03*, Wallingford, CT: Gaussian Inc., (2016).
[58] H. M. Pickett, J. Mol. Spectrosc. **148**, 371 (1991).
[59] J. K. Watson, in *Vibrational Spectra and Structure*, J. R. Durig Ed., New York: Elsevier, (1977).
[60] Z. Kisiel, J. Mol. Spectrosc. **218**, 58 (2003).
[61] D. Millen, Can. J. Chem. **63**, 1477 (1985).

DOI: 10.1063/1674-0068/cjcp2309082